

The latest Aptian / earliest Albian age of the Kekura gold deposit, Western Chukotka, Russia: Implications for mineralization associated with post-collisional magmatism

Ekaterina V. Nagornaya^{1,2}, Ivan A. Baksheev², David Selby^{3,4}, Petr L. Tikhomirov^{2,5}

¹Vernadsky Institute of Geochemistry and Analytical Chemistry RAS, 19 Kosygin str., Moscow 119991, Russia

²Faculty of Geology, Lomonosov Moscow State University, GSP-1, Leninskie Gory, Moscow 119991, Russia

³Department of Earth Sciences, Durham University, Durham DH1 3LE, UK

⁴State Key Laboratory of Geological Processes and Mineral Resources, School of Earth Resources, China University of Geosciences, Wuhan 430074, China

⁵North-East Interdisciplinary Scientific Research Institute, 16 Portovaya str., Magadan 685000, Russia

Corresponding author: Ekaterina V. Nagornaya chp312@gmail.com

ORCID:

Ekaterina V. Nagornaya 0000-0002-9083-5380

Ivan A. Baksheev 0000-0001-6920-427X

David Selby 0000-0001-9798-2351

Petr L. Tikhomirov 0000-0002-0232-360X

Abstract. The Kekura gold deposit (76.2 t Au at 8.1 g/t) is situated in Western Chukotka, a region that hosts several Au, Ag, Cu, and Mo deposits and prospects. The Kekura deposit is related to the eponymous granite intrusion that is cut by porphyry dikes. The U-Pb zircon age of one of these dikes is 112 ± 1 Ma (2σ) that corresponds to the latest Aptian / earliest Albian. Both intrusion and dikes are hydrothermally altered and are cut by gold-quartz and molybdenite-quartz veins and stringers. Two molybdenite samples yield Re-Os model ages of 112.5 ± 0.6 and 112.3 ± 0.6 Ma (2σ). These Re-Os ages indicate the close temporal relationship between the molybdenite mineralization and the porphyry dikes. The age of the Kekura mineral system is similar to that of the post-collisional granitic plutons of the Anyui zone spatially scattered, between 140 and 210 km northwest of Kekura. We suggest that this temporal relationship may increase the likelihood of further discoveries of economic gold mineralization related to the currently underexplored Aptian post-collisional magmatic complexes of the Western Chukotka area.

Keywords: zircon, U-Pb geochronology, molybdenite, Re-Os geochronology, Kekura deposit, Western Chukotka

Introduction

The Western Chukotka region of Russia is host to several gold, silver, copper, and molybdenum deposits and prospects. Amongst them are the Kupol (55.3 t Au at 36.4 g/t, 752 t Ag at 485.7 g/t; Vasil'kova et al. 2018) and Dvoinoe (28.1 t Au at 2.3 g/t; Vasil'kova et al. 2018) epithermal gold-silver deposits, the Karalveem intrusion-related gold deposit (9.1 t Au at 14.1 g/t; Akimova et al. 2016), the Klen intermediate sulfidation epithermal gold deposit (18.6 t Au at 5 g/t; www.russdragmet.ru), and the Peschanka (3.7 Mt Cu at 0.83%, 98 kt Mo at 230 g/t, 234 t Au at 0.57 g/t, 2002 t Ag at 4.6 g/t; Vasil'kova et al. 2018) and Nakhodka (3.1 Mt Cu at 0.34%, 50 kt Mo at 54 g/t, 278 t Au at 0.30 g/t, 1130 t Ag at 1.2 g/t; Chitalin et al. 2013) porphyry copper deposits.

The available zircon U-Pb data (Akinin et al. 2015; Nikolaev et al. 2016) indicate that magmatism associated with mineralization highlights three major magmatic-hydrothermal events at 144–138 Ma (represented by the Peschanka and Nakhodka porphyry Cu-Au-Mo systems), 120–118 Ma (e.g., Dvoinoe epithermal deposit), and 97–92 Ma (e.g., Kupol epithermal deposit). However, both magmatic evolution and mineralization of Western Chukotka remain poorly studied, especially in terms of precise geochronology.

The Kekura hydrothermal gold deposit is situated approximately 120 km southwest of the town of Bilibino, Chukotka Autonomous Area, Russia (Fig. 1a). Kekura was discovered in 1990 by a team of the Anyui Exploration Expedition. Further assessment of the mineralization at Kekura was carried out by the Sibir Mining Company between 2004 to 2010. The deposit is currently owned by Highland Gold Mining Limited and is set to go into production in 2023. According to Highland Gold Mining, Kekura hosts a large JORC compliant resource base of 76.2 t at a grade of 8.1 g/t (www.highlandgold.com).

Available information on the geology and mineralization at Kekura is limited and to date has only been published in abstract-form at various conferences (Dvurechenskaya et al. 2007; Baksheev et al. 2015, 2019). Currently there are no published data on the age of igneous rocks and mineralization at Kekura. Here, we present the first dating of magmatism and mineralization of the Kekura deposit via U-Pb zircon geochronology of a hydrothermally altered granodiorite porphyry dike and Re-Os molybdenite dating of disseminated molybdenite and quartz-molybdenite veinlets hosted by the granodiorite porphyry. We demonstrate that the Kekura deposit formed during the latest Aptian / earliest Albian associated with post-collisional magmatic activity, which postdates the formation of the South Anyui suture. The results also provide a scientific basis for future mineral exploration in this region.

Geology and mineralization

The West Chukotka area comprises four major tectonic zones (from SW to NE; see Fig. 1b): (1) the marginal part of the Omolon cratonic terrane; (2) the Oloy zone, dominated by Jurassic and Early Cretaceous continental (?) arc magmatism; (3) the South Anyui suture zone, formed in the Early Cretaceous, after the closure of an oceanic basin and subsequent collision between the Chukotka block and the Siberian continent, and (4) the Anyui zone, the former passive margin of the Chukotka block (Parfenov 1991; Nokleberg et al. 2001). All four zones have been overprinted by a post-collisional magmatic event at ca. 121–112 Ma (Tikhomirov et al. 2017; Kara et al. 2019), and later by subduction-related volcanism of the Okhotsk-Chukotka volcanic belt (106–74 Ma; Akinin and Miller 2011; Tikhomirov et al. 2012).

The Oloy zone hosts the large Peschanka and Nakhodka porphyry Cu-Au-Mo deposits, the small minor Mangazeika porphyry Cu-Mo-Au and the Klen intermediate sulfidation epithermal gold deposit. The large Karalveem intrusion-related gold deposit is situated in the Anyui tectonic zone. The Kekura deposit, the subject of this study, is located in the South Anyui zone.

The South Anyui zone stretches for ~600 km and has a width of 15 to 40 km. It is characterized by a series of NW-SE trending tectonic slices composed by intensely folded clastic rocks that are occasionally intercalated with basalts and cherts. The age of the volcanic and sedimentary rocks of the South Anyui zone ranges from Late Triassic to Early Cretaceous (Sokolov et al. 2009). The youngest detrital zircons extracted from the clastic rocks of the zone yield U-Pb ages of ca. 125 Ma (Amato et al. 2015), suggesting that final orogenic collision occurred during the early Aptian.

The Kekura deposit area (Fig. 2; ESM Fig. 1) comprises a Late Triassic highly deformed flysch-like sequence composed of folded and fractured intercalated mudstone, siltstone, sandstone. This sequence is intruded by the Kekura three-phase granitic pluton that is considered part of the Early Cretaceous Gvardeisky Igneous Complex. Mineralization of the deposit is spatially related to intrusive rocks. Bulk-rock K-Ar age determinations for the Gvardeisky complex range from 124 to 94 Ma (Furman 1999), suggesting a likely Early Cretaceous age for magmatism. The outcrop area of the Kekura stock is about 13 km² and is represented by three phases of magmatism. Based on cross cutting relationships these are (oldest to youngest) medium-grained diorite, medium- to coarse-grained quartz monzodiorite and syenite, and medium- to coarse-grained granodiorite. The igneous rocks contain xenoliths of gabbro. The Kekura pluton has not been affected by any considerable compressional tectonic event, but is cut by numerous and multi-directional dikes of pre-ore granodiorite and granite porphyries, and spessartite, and a post-ore diorite porphyry.

Mineralization is represented by several stages. Stage 1 is characterized by Ni-Co-Fe arsenides and sulfoarsenides (nickeline, safflorite, cobaltite, löllingite) and native bismuth. Stage 2 is represented by molybdenite, bornite, chalcopyrite, and pyrite I. The bulk of the economic mineralization (Stage 3) includes two substages. The first substage is represented by scheelite, arsenopyrite, pyrite II, chalcopyrite II, sphalerite, galena, tennantite-tetrahedrite, maldonite, and native gold (fineness approximately 850). The second substage of Stage 3 mineralization is characterized by Bi tellurides and

sulfotellurides, native bismuth, bismuthinite, and gold with fineness of 920–995 as a decomposition product of maldonite. The final mineralization Stage 4 is characterized by chalcopyrite III, galena II, boulangerite, bournonite, Ag-rich tetrahedrite, Sb-bearing sphalerite, stibnite, low fineness Au-Ag alloy, and native silver. Each mineralization stage is characterized by a distinct hydrothermal alteration assemblage. A propylitic assemblage of quartz-oligoclase-actinolite-clinocllore-calcite is common to Stage 1 mineralization. An albite-quartz-muscovite-tourmaline assemblage is associated with Stage 2 mineralization. The Stage 3 mineralization episode is associated with an alteration assemblage of quartz-dolomite-muscovite and arsenopyrite. The Stage 4 mineralization is associated with a muscovite-illite-siderite-quartz assemblage.

Sample description

Two samples of granodiorite porphyry dikes were collected from surface exposures (Fig. 2). The outcropping porphyry is altered to a yellowish, medium-grained quartz-carbonate-muscovite rock. The porphyry dike is cut by Stage 2 quartz-molybdenite veinlets up to 1 cm wide and hosts disseminated molybdenite as rosettes up to a few cm in size (ESM Fig. 2).

Sample 66842-40168 is massive granodiorite porphyry with a fine-crystalline matrix that is cut by numerous carbonate and quartz stringers. Phenocrysts of primary magmatic minerals are plagioclase (60%), quartz (20%), potassium feldspar (10%), and biotite and highly altered amphibole (10%). Apatite, zircon, and ilmenite are accessory minerals. Phenocrysts of primary plagioclase and potassium feldspar occur as up to 2 mm tabular crystals. Plagioclase is partly replaced by saussurite and albite. Potassium feldspar exhibits weak argillic alteration. Rounded subhedral to anhedral quartz phenocrysts of up to 2 mm are not altered. Primary biotite of up to 0.5 mm is completely replaced by an assemblage of rutile-muscovite-chlorite and carbonate. The groundmass (65% of the sample) is composed of potassium feldspar, primary magmatic quartz, plagioclase, biotite, and hornblende, and is partially replaced by albite, muscovite, dolomite, and chlorite. This sample also contains a Stage 2 10 mm wide quartz-molybdenite vein (ESM Fig. 2a), with the molybdenite being a few hundred microns in length. The sample was utilized for both U-Pb zircon and Re-Os molybdenite dating.

Sample 4015-6605 is massive granodiorite porphyry with a fine-crystalline matrix. Phenocrysts are predominantly plagioclase (70%), quartz (20%), and potassium feldspar and biotite (10%). Zircon, apatite, and ilmenite are accessory minerals. Plagioclase phenocrysts up to 2.5 mm are partly replaced by sericite and albite. Subhedral quartz, up to 2 mm, is unaltered. Up to 2 mm anhedral potassium feldspar exhibit argillic alteration. Biotite phenocrysts (up to 1 mm) are altered to sericite and rutile. The fine-grained groundmass (60% of the sample) of quartz, plagioclase, potassium feldspar, biotite, and hornblende is significantly altered to albite, muscovite and dolomite. Thin (5–10 mm) quartz-

carbonate-sericite stringers also cut the rock. Fine grained (few hundred microns in length) molybdenite is present as disseminated rosettes (up to a few cm in size) throughout the groundmass of the granodiorite porphyry (ESM Fig. 2b). Molybdenite from this sample was utilized for Re-Os dating.

Methods

U-Pb zircon dating. Zircons from sample 66842-40168 were analyzed at the Centre of Isotopic Research of the Russian Geological Institute, St. Petersburg, Russia. Separated grains of zircon were handpicked, mounted in epoxy resin randomly oriented together with mineral standards, and polished until the crystal centers of the grains were exposed. Potential target sites for the isotope analyses were carried out using a CamScan-2500 electron microprobe together with reflected and transmitted light microscopy. Back-scattered electron (BSE) and cathodoluminescence (CL) images of grains were obtained in order to assess internal compositional variation and their textures; moreover, in addition SEM-EDX information about mineral inclusions was ascertained.

The U-Th-Pb isotope analyses were conducted by secondary ion microprobe (SHRIMP-II) instrument with pit diameter ca 40 μm , corresponding primary O^{2-} beam intensity was about 9 nA. The zircon ages were calculated from $^{206}\text{Pb}/^{238}\text{U}$ measured ratios which have been normalized relative to a value of 0.0668 for the $^{206}\text{Pb}/^{238}\text{U}$ ratio of the TEMORA reference zircons, equivalent to an age of 416.75 Ma (Black et al. 2003). Individual analysis consisted of five cycles (150 sec per cycle), each cycle representing one pass through the mass stations: $^{196}(\text{Zr}_2\text{O})$, ^{204}Pb , 204 background, ^{206}Pb , ^{207}Pb , ^{208}Pb , ^{238}U , $^{248}(\text{ThO})$, $^{254}(\text{UO})$. The U-Pb data were processed in a manner described by Baldwin and Ireland (1995). Assuming concordance of ages, the mixing line between common and radiogenic portions was plotted. The lower interception of this line with concordia gives an age of the zircons. The Th-Pb ages were determined from $^{208}\text{Pb}/^{232}\text{Th}$ ratios through the common U-Th-Pb SHRIMP procedure (Williams 1998), corrected for any common lead content detected from ^{204}Pb . The U and Th content was normalized relative to the 91500 zircon reference standard. The obtained isotope data were processed using the SQUID-1 program (Ludwig 2000), with concordia diagrams plotted using ISOPLOT/EX (Ludwig 2003).

Re-Os molybdenite dating. Two molybdenite samples, obtained from samples 66842-40168 and 4015-6605, were analyzed in the Source Rock and Sulfide Geochemistry and Geochronology, and Arthur Holmes Laboratories at University of Durham (United Kingdom) to establish the Re-Os age of molybdenite mineralization. Molybdenite separation was achieved through using traditional methods (crushing to 70 to 200 mesh, magnetic separation, heavy liquids and final hand picking to remove any impurities). For both samples, no other ore minerals are present together with the molybdenite. An aliquant of the molybdenite separate (~20 mg) together with a known amount of tracer solution (^{185}Re + Os bearing a normal isotope composition) were placed into a carius tube and digested with 3mL HCl and 6mL HNO_3 at 220°C for 23

hrs. Osmium was isolated and purified using solvent extraction (CHCl_3) and microdistillation methods, with the resulting Re-bearing fraction purified using NaOH-Acetone solvent extraction and anion chromatography (Selby and Creaser 2004; Li et al. 2017). Although negligible in comparison to the Re and Os abundance in the molybdenite, the final Re-Os data are blank corrected. A full analytical protocol blank run parallel with the molybdenite analysis yields 4.1 pg Re and 0.7 pg Os, the latter possessing a $^{187}\text{Os}/^{188}\text{Os}$ composition of 0.20 ± 0.2 . Data treatment follows that outlined in Li et al. (2017). All Re-Os data are given with 2σ absolute uncertainties (Table 1). Molybdenite Re-Os ages are calculated using a ^{187}Re decay constant of $1.666 \times 10^{-11} \text{ y}^{-1}$ with an uncertainty of 0.31% (Smoliar et al. 1996; Selby et al. 2007). The Henderson molybdenite reference material (RM8599) analyzed during the course of this study yields a Re-Os age of $27.78 \pm 0.11 \text{ Ma}$ (2σ ; $n = 1$), which is in good agreement with the recommended value of $27.66 \pm 0.10 \text{ Ma}$ (Markey et al. 2007; Zimmerman et al. 2014), and that reported by Li et al. (2017; $27.695 \pm 0.038 \text{ Ma}$, $n = 9$) and previous analysis at Durham (e.g., $27.65 \pm 0.12 \text{ Ma}$; Lawley and Selby 2012 and references therein).

Results

U-Pb dating of granodiorite porphyry. Ten zircon grains from porphyry granodiorite dike sample 66842-40168 analyzed in this study are colorless to possessing a yellowish tint. All zircons are transparent, euhedral to subhedral, elongate, and contain minor fractures. The zircons also contain melt and unidentified mineral inclusions (ESM Fig. 3a). The zircon grains show magmatic fine oscillatory zoning parallel to the crystal faces (ESM Fig. 3b). Evidence for zircon inheritance is absent.

The U and Th concentrations in the zircon grains range from 231 to 652 ppm and from 98 to 472 ppm, respectively. The Th/U ratios are between 0.34 and 0.82. Their common Pb concentrations vary from being below the detection limit to 1.57 ppm (ESM Table 1). All U-Pb data plot near the concordia line, and yield a $^{238}\text{U}/^{206}\text{Pb}$ age of $111.0 \pm 2.0 \text{ Ma}$ (MSWD = 6.6, 2σ) (Fig. 3a). A $^{238}\text{U}/^{206}\text{Pb}$ ages yield a weighted average of $112.0 \pm 1.0 \text{ Ma}$ (MSWD = 0.46; Fig. 3b). These ages correspond to the latest Aptian / earliest Albian and are taken to be the best estimate for timing of emplacement of the porphyry granodiorite.

Re-Os molybdenite dating. The Re and ^{187}Os concentrations of the two molybdenite samples studied are similar: Re = 98.0 and 104.7 ppm; ^{187}Os = 115.4 and 123.4 ppb, respectively (Table 1). The Re-Os model ages for both samples are identical within uncertainty: sample 4015-6605 = $112.5 \pm 0.6 \text{ Ma}$; sample 66842-40168 = $112.3 \pm 0.6 \text{ Ma}$.

Discussion

The dated granodiorite porphyry is host to the dated quartz-molybdenite bearing vein and disseminated molybdenite. The Re-Os molybdenite ages of 112.5 ± 0.6 and $112.3 \pm 0.6 \text{ Ma}$ are identical within uncertainty to the zircon

$^{238}\text{U}/^{206}\text{Pb}$ weighted average age of the granodiorite porphyry (112.0 ± 1.0 Ma). These ages indicate that the molybdenum (Stage 2) mineralization of the Kekura deposit is temporally related to the magmatism associated with the granodiorite porphyry dike. Further it constrains magmatism and mineralization to the Late Aptian / Early Albian likely being related to the third intrusion phase of the Kekura pluton.

The isotopic age of the Kekura deposit does not correspond to any of three known mineralization epochs in the Western Chukotka area (144–138, 120–118, and 97–94 Ma; Akinin et al. 2015; Nikolaev et al. 2016). Uranium-Pb zircon ages of 117 to 112 Ma have been reported for several post-collisional granitic plutons of the Anyui zone (Miller et al. 2009), which occur between 140 and 210 km northwest of Kekura (Fig. 1b). These plutons are considered to be part of an Aptian post-collisional magmatic event present in the West Chukotka area (Tikhomirov et al. 2017; Kara et al. 2019). Linking the Kekura deposit to the Aptian magmatic event increases the duration of the Aptian metallogenic epoch (120–118 Ma), and implies that both epithermal and intrusion-related gold deposits were formed during this time period.

Alternatively, the Kekura pluton and related gold mineralization could be linked to the next magmatic pulse of Albian age. Zircon U-Pb dates of 109 to 105 Ma have been obtained for granitic batholiths and smaller plutons of North Chukotka (Miller and Verzhbitsky 2009; Tikhomirov et al. 2011; Luchitskaya et al. 2019). Similar U-Pb ages (109.3 ± 1.2 Ma, 108.5 ± 2.7 Ma, and 100.9 ± 0.8 Ma) have been reported for post-tectonic plutons and dikes of the South Anyui zone (Miller et al. 2009; Amato et al. 2015). The earliest formations of the huge subduction-related Okhotsk-Chukotka volcanic belt return $^{40}\text{Ar}/^{39}\text{Ar}$ and U-Pb ages of ca. 106 Ma (Akinin and Miller 2011; Tikhomirov et al. 2012). Further, plutons in the northern Chukotka region host several large tin deposits (Flerov 1976), but any genetic relationship between gold mineralization and Albian magmatism is yet to be shown.

The hypothesis linking the Kekura deposit to the Aptian magmatic event looks more plausible because the isotopic age of the Kekura deposit is somewhat closer to the age of Aptian magmatic pulse than that known for the Albian event. Besides, the formation of intrusion-related gold deposits is commonly restricted to the relatively late stages of major magmatic events (Lang and Baker 2001). In addition, the new ages for the post-tectonic Kekura pluton indicate that the late stages of major deformation in the South Anyui zone took place prior to ca. 112 Ma.

Conclusions

This study reports the first U-Pb and Re-Os ages for zircon of a porphyry granodiorite dike and molybdenite disseminated within the dyke and hosted by quartz veins cross cutting the dike, respectively from the Kekura gold deposit, Chukchi Peninsula, Russia. The precise U-Pb zircon age of 112 ± 1 Ma and Re-Os molybdenite ages of 112.5 ± 0.6 and 112.3 ± 0.6 Ma are essentially identical within uncertainty and show that hydrothermal molybdenite mineralization is genetically related to the timing of the granodiorite porphyry dike and the gold mineralization. The U-Pb and Re-Os ages

reported here document the latest Aptian / earliest Albian age for the granodiorite porphyry and associated molybdenum mineralization at the Kekura gold deposit. The ages obtained are close to some of the post-collisional granite plutons in the Anyui tectonic zone. The spatial relationship between gold mineralization and post-collisional Aptian magmatic rocks in the Western Chukotka implies that there are very likely understudied fragments of magmatic-volcanic fields of presumably Aptian age, which are widespread across the western Oloy zone and NE Omolon block that could potentially host significant economic mineral systems.

Acknowledgements

The study was funded by Russian Foundation for Basic Research according to the research project No. 18-35-20034. The work by P.L. Tikhomirov was supported by NEISRI Research Program (0288-2017-0002) and Far East Branch of RAS (grant 18-2-015). David Selby acknowledges the Total Endowment Fund and a CUG (Wuhan) scholarship. We thank Highland Gold Mining Limited for the access to samples and the Centre of Isotopic Research at VSEGEI for performing the zircon dating. Yulia Khabibullina, Maria Volkova, Antonia Hofmann, Geoff Nowell and Chris Ottley are acknowledged for technical support. The authors also would like to sincerely thank Prof. Dr. Bernd Lehmann for reading the manuscript, correcting it and for his constructive comments and suggestions which resulted in greatly improving it. Thanks are also extended to the anonymous reviewer for their constructive suggestions and comments.

References

- Akimova AV, Vasil'kova NA, Dorozhkina LA et al (2016) On the state and use of mineral resources of the Russian Federation in 2015. Report of the Ministry of Natural Resources and Ecology of the Russian Federation. VIMS, Mineral, Moscow [in Russian]
- Akinin VV, Miller EL (2011) Evolution of calc-alkaline magmas of the Okhotsk-Chukotka volcanic belt. *Petrology* 19:237–277
- Akinin VV, Thomson B, Polzunenkov GO (2015) U-Pb and $^{40}\text{Ar}/^{39}\text{Ar}$ dating of magmatism and mineralization at the Kupol and Dvoinoe gold deposits. *Isotope dating of geologic processes: new results, approaches, and prospects: Proceedings of the VI All-Russia conference on isotope geochronology*. St Petersburg, IGGD RAN, pp. 19–21

Amato JM, Toro J, Akinin VV, Hampton BA, Salnikov AS, Tuchkova MI (2015) Tectonic evolution of the Mesozoic South Anyui suture zone, eastern Russia: A critical component of paleogeographic reconstructions of the Arctic region. *Geosphere* 11:1530–1564

Baksheev IA, Demin AD, Bryzgalov IA, Marushchenko LI, Prokofiev VY, Nikolaev YN, Kosyatov VV (2015) Mineralogy of wall-rock alterations and ores at the Kekura gold deposit, Western Chukchi Peninsula, Russia. Proceedings of the VIII International symposium “Mineral Diversity: Research and Preservation”, Sofia, Bulgaria, p. 20

Baksheev IA, Nagornaya EV, Komarova MM, Khabibullina YN, Kalko IA (2019) Fluid inclusion study in quartz vein of the Kekura gold deposit, Western Chukchi Peninsula, Russia. *Acta Mineral-Petrogr* 10:15

Baldwin SL, Ireland TR (1995) A tale of two eras: Pliocene-Pleistocene unroofing of Cenozoic and Late Archean zircons from active metamorphic core complexes, Solomon Sea, Papua New Guinea. *Geol* 23:1023–1026

Black LP, Kamo SL, Allen CM, Aleinikoff JN, Davis DW, Korsch RJ, Foudoulis C (2003) TEMORA 1: a new zircon standard for Phanerozoic U-Pb geochronology. *Chem Geol* 200:155–170

Chitalin AF, Usenko VV, Fomichyov YV (2013) The Baimskaya ore zone — a cluster of large deposits of non-ferrous and precious metals in the west of the Chukotka autonomous district. *Mineral Resources of Russia, Economics & Management* 6:68–73 [in Russian]

Dvurechenskaya SS, Kryazhev SG, Nurgaliev GN, Elmanov AA (2007) Mineralogy of the Kekura gold deposit (Chukotka). Russian Miner Soc Ann Session “Mineralogical Investigations and Mineral Resources of Russia”, Vol. 2007-2, pp. 23–26 [in Russian]

Flerov BL (1976) Tin deposits of Yana-Kolyma tectonic province. Nauka, Novosibirsk [in Russian]

Furman OA (1999) Legend for the Oloy map series of State geological map of Russian Federation, scale 1:200000. Bilibino, Anyuiskoe GGGP. [in Russian]

- Kara TV, Tikhomirov PL, Demin AD (2019) New data on the age of magmatic events in the Oloi fold zone, Western Chukotka: evidence from U-Pb zircon dating. *Dokl Earth Sci* 489:911–916
- Lang JR, Baker T (2001) Intrusion-related gold deposits: the present level of understanding. *Miner Deposita* 36:477–489
- Lawley CJM, Selby D (2012) Re-Os geochronology of quartz enclosed ultra-fine molybdenite: Implications for ore geochronology. *Econ Geol* 107(7):1499–1506
- Li Y, Li X-H, Selby D, Li J-W (2017) Pulsed magmatic fluid release for the formation of porphyry deposits: Tracing fluid evolution in absolute time from the Tibetan Qulong Cu-Mo deposit. *Geol* 46:7–10
- Luchitskaya MV, Sokolov SD, Verzhbitsky V, Vatrushkina EV, Ganelin AV, Golionko B (2019) Roles of postcollisional granitoids and Aptian–Albian extension in tectonic evolution of Mesozoic structures on Chukchi Peninsula, Northeastern Russia. *Dokl Earth Sci* 484:48–52
- Ludwig KR (2000) SQUID 1.00. A user's manual. Berkeley Geochronology Special Publication 2
- Ludwig KR (2003) User's Manual for Isoplot/Ex, Version 3.00, A Geochronological Toolkit for Microsoft Excel. Berkeley Geochronology Center Special Publication 1a
- Markey R, Stein HJ, Hannah JL, Zimmerman A, Selby D, Creaser RA (2007) Standardizing Re-Os geochronology: a new molybdenite Reference Material (Henderson, USA) and the stoichiometry of Os salts. *Chem Geol* 244:74–87
- Miller EL, Katkov SM, Strickland A, Toro J, Akinin VV, Dumitru TA (2009) Geochronology and thermochronology of Cretaceous plutons and metamorphic country rocks, Anyui-Chukotka fold belt, North East Arctic Russia. *Stephan Mueller Spec Publ Ser* 4:157–175
- Miller EL, Verzhbitsky VE (2009) Structural studies near Pevek, Russia: implications for formation of the East Siberian Shelf and Makarov Basin of the Arctic Ocean. *Stephan Mueller Spec Publ Ser* 4:223–241

- Nikolaev YN, Baksheev IA, Prokofiev VY, Nagornaya EV, Marushchenko LI, Sidorina YN, Chitalin AF, Kal'ko IA (2016) Gold–Silver Mineralization in Porphyry–Epithermal Systems of the Baimka Trend, Western Chukchi Peninsula, Russia. *Geol Ore Deposits* 58:284–307
- Nokleberg WJ, Parfenov LM, Monger JWH, Norton IO, Khanchuk AI, Stone DB, Scotese CR, Scoll DW, Fujita K (2001) Phanerozoic tectonic evolution of the Circum-North Pacific. US Geological Survey Professional paper 1626
- Parfenov LM (1991) Tectonics of the Verkhoyansk-Kolyma Mesozoides in the context of plate tectonics. *Tectonophys* 199:319–342
- Selby D, Creaser RA (2004) Macroscale NTIMS and microscale LA-MC-ICP-MS Re-Os isotopic analysis of molybdenite: Testing spatial restrictions for reliable Re-Os age determinations, and implications for the decoupling of Re and Os within molybdenite. *Geochim Cosmochim Acta* 68:3897–3908
- Selby D, Creaser RA, Stein HJ, Markey RJ, Hannah JL (2007) Assessment of the ^{187}Re decay constant by cross calibration of Re-Os molybdenite and U-Pb zircon chronometers in magmatic ore systems. *Geochim Cosmochim Acta* 71:1999–2013
- Smoliar MI, Walker RJ, Morgan JW (1996) Re-Os isotope constraints on the age of Group IIA, IIIA, IVA, and IVB iron meteorites. *Science* 271:1099–1102
- Sokolov SD, Bondarenko GY, Layer PW, Kravchenko-Berezhnoy IR (2009) South Anyui suture: tectono-stratigraphy, deformations, and principal tectonic events. *Stephan Mueller Spec Publ Ser* 4:201–221
- Tikhomirov PL, Kalinina EA, Moriguti T, Makishima A, Kobayashi K, Cherepanova IY, Nakamura E (2012) The Cretaceous Okhotsk-Chukotka Volcanic Belt (NE Russia): Geology, geochronology, magma output rates, and implications on the genesis of silicic LIPs. *J Volcanol Geoth Res* 221–222:14–32
- Tikhomirov PL, Luchitskaya MV, Shats AL (2011) Age of granitoid plutons, North Chukotka: Problem formulation and new SHRIMP U-Pb zircon datings. *Dokl Earth Sci* 440:1363–1366

Tikhomirov PL, Prokof'ev VY, Kal'ko IA, Apletalin AV, Nikolaev YN, Kobayashi K, Nakamura E (2017) Post-collisional magmatism of Western Chukotka and Early Cretaceous tectonic rearrangement in northeastern Asia. *Geotectonics* 51:131–151

Vasil'kova NA, Goreva AA, Danil'chenko VA et al (2018) On the state and use of mineral resources of the Russian Federation in 2016 and 2017. Report of the Ministry of Natural Resources and Ecology of the Russian Federation, VIMS, Mineral, Moscow [in Russian]

Williams IS (1998) U-Th-Pb geochronology by ion microprobe. In: McKibben MA., Shanks III WC, Ridley WI (eds) *Applications of Microanalytical Techniques to Understanding Mineralizing Processes*. *Rev Econ Geol* 7:1–35

Zimmerman A, Stein HJ, Morgan JW, Markey RJ, Watanabe Y (2014) Re-Os geochronology of the El Salvador porphyry Cu-Mo deposit, Chile: Tracking analytical improvements in accuracy and precision over the past decade: *Geochim Cosmochim Acta* 131:13–32

Figure captions

Fig. 1 Location of the Kekura gold deposit and tectonic map of Western Chukotka, modified after Tikhomirov et al. (2017). Numbers with the names of the deposits depict the time span of deposit formation in Ma determined by radiometric dating (data from Akinin et al. 2015, Nikolaev et al. 2016 and references therein, this study)

Fig. 2 Geological map of the Kekura gold deposit and sample locations. Solid grey circle corresponds to granodiorite sample 66842-40168 for zircon U-Pb dating and molybdenite Re-Os dating; solid black circle represents sample 4015-6605 for molybdenite Re-Os dating

Fig. 3 SIMS U/Pb zircon isotope plots from porphyry granodiorite sample 66842-40168: (a) $^{238}\text{U}/^{206}\text{Pb}$ vs. $^{207}\text{Pb}/^{206}\text{Pb}$ concordia plot and (b) weighted average $^{238}\text{U}/^{206}\text{Pb}$ age plot

Table 1 Re-Os data of molybdenite from the Kekura gold deposit and the molybdenite reference material RM8599

Sample	wt (g)	Re (ppm)	±	¹⁸⁷ Re (ppm)	±	¹⁸⁷ Os (ppb)	±	Age (Ma)	± [^]	± [*]	± [#]
66842-40168	0.021	98.0	0.4	61.6	0.2	115.4	0.4	112.3	0.1	0.5	0.6
4015-6605	0.022	104.7	0.4	65.8	0.2	123.4	0.4	112.5	0.1	0.5	0.6
RM8599	0.100	11.01	0.0	6.9	0.0	3.2	0.0	27.8	0.0	0.1	0.1

All uncertainties quoted are 2σ absolute.

[^]uncertainty including only mass spectrometry uncertainty

^{*}uncertainty including all sources of analytical uncertainty

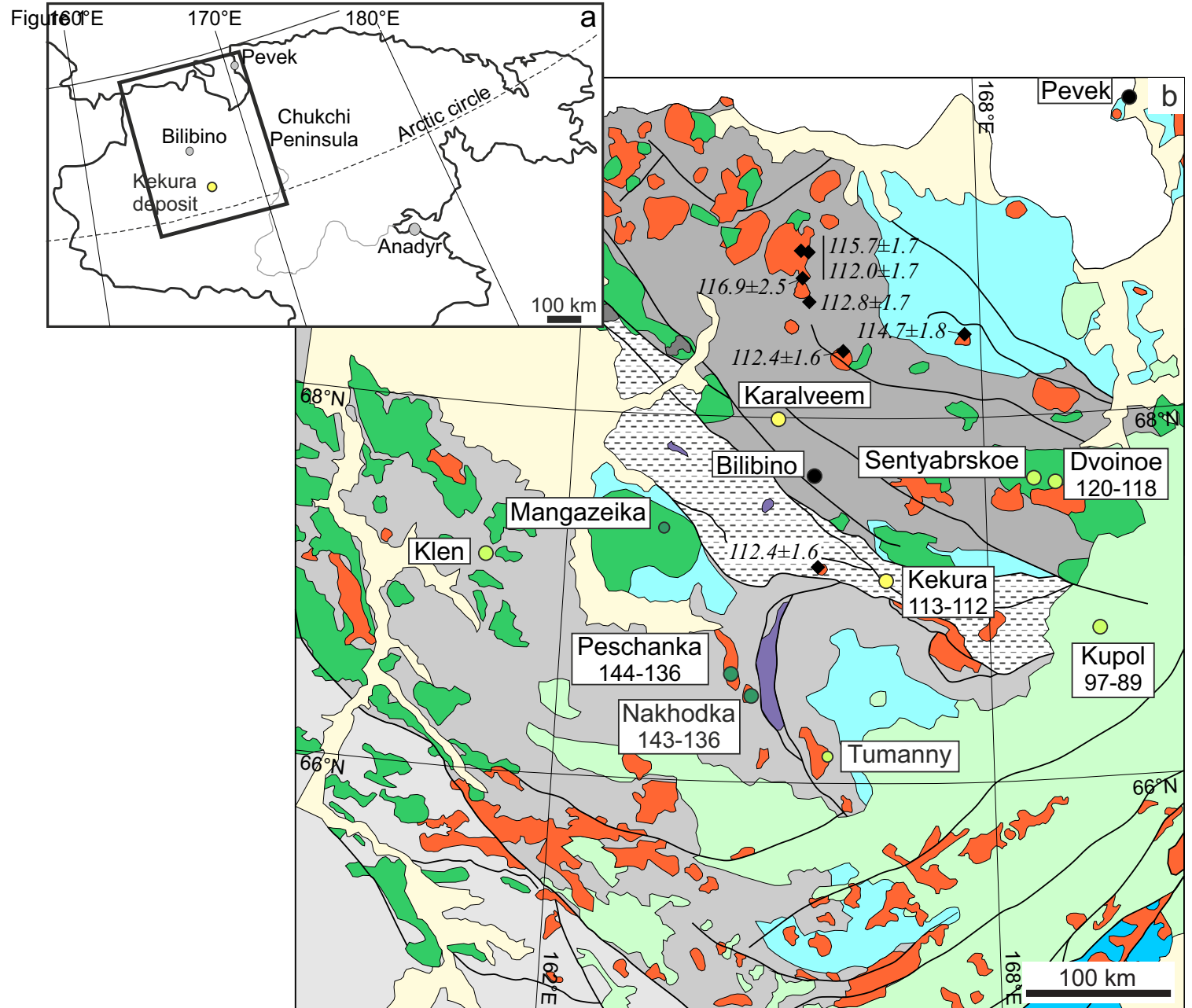
[#]uncertainty including all sources of analytical uncertainty plus decay constant

ESM Fig. 1 A field photograph looking east over the Kekura deposit area. The dashed line partly outlines the mineralized outcrop

ESM Fig. 2 Photographs of molybdenite-bearing samples of the altered granodiorite porphyry: (a) sample 66842-40168 – quartz-molybdenite vein and (b) sample 4015-6605 – disseminated molybdenite

ESM Fig. 3 Images of zircon grains from granodiorite porphyry sample 66842-40168: (a) photograph of zircon grains under an optical binocular microscope and (b) cathodoluminescent image of the zircon grains showing the oscillatory zoning parallel to the crystal faces and the position of the secondary ion microprobe (SHRIMP-II) analyses

ESM Table 1 U-Pb data for zircons from sample 66842-40168 from the Kekura gold deposit



Tectonic zones of the Verkhoyansk-Chukotka province

Omolon (a slightly deformed cover of Paleozoic and Mesozoic clastic and volcanic strata over the Precambrian crystalline basement)

Oloy (tectonic collage of Paleozoic and Mesozoic active margin complexes)

South Anyui (suture zone formed after the closure of an oceanic basin; strongly deformed Mesozoic clastic and volcanic strata)

Anyui (Late Permian(?) through Triassic clastic complexes of the passive margin of Chukotka continental block)

Late Jurassic through Early Cretaceous syn-collisional and post-collisional basins filled with clastic sediments

Massifs of Paleozoic ophiolitic gabbro and peridotites

Granitic plutons, dominantly Cretaceous

Post-collisional volcanic complexes (Aptian)

Uda-Murgal belt (Late Jurassic through Early Cretaceous)

Okhotsk-Chukotka belt (Albian through Campanian)

Quaternary sediments

Major faults

Subduction-related volcanic belts

Cu-Mo-Au porphyry deposit

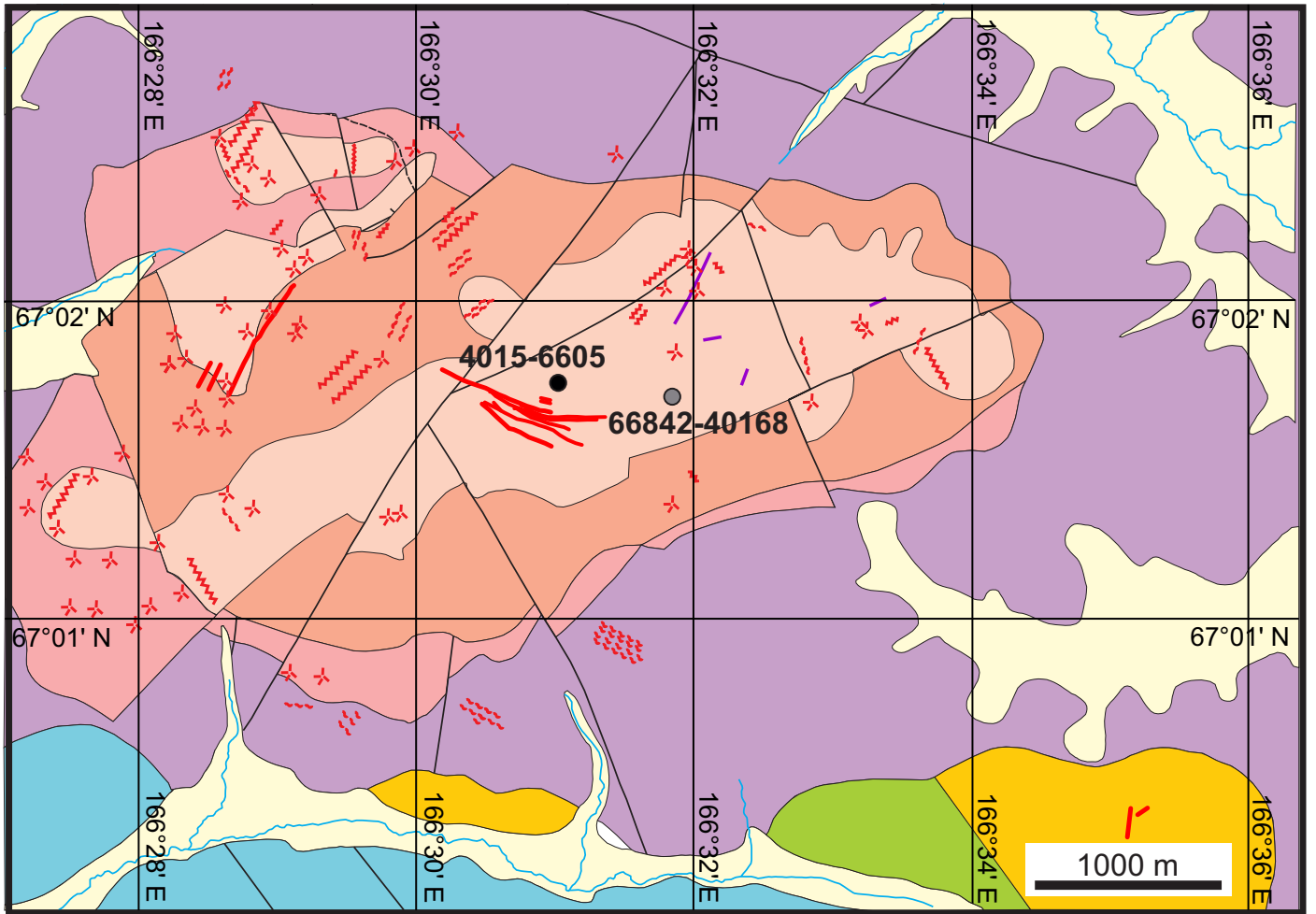
Au granitoid-related deposit

Au-Ag IS / LS epithermal prospect and deposit

Approximate location and U-Pb age ($\pm 2\sigma$) of granitic samples from Anyui and South Anyui zones (Miller et al. 2009)

115.7 \pm 1.7

Figure 2



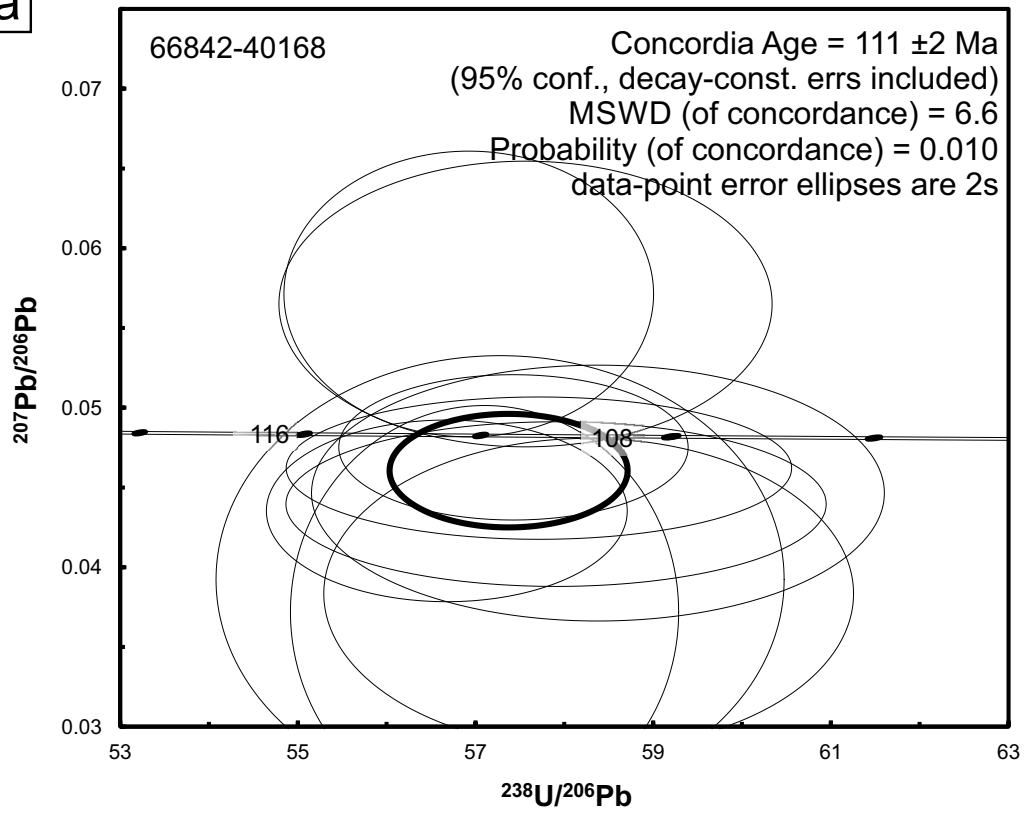
- Quaternary alluvium
- Early Cretaceous siltstone, sandstone, rare gravelstone, intercalated tuff and tuffite
- Late Jurassic siltstone and sandstone
- Late Triassic flysch-like intercalated mudstone, siltstone, arcose, and sandstone
- Permian andesitic tuff, tuffite, and tuffaceous conglomerate

Early Cretaceous Gvardeisky Igneous Complex

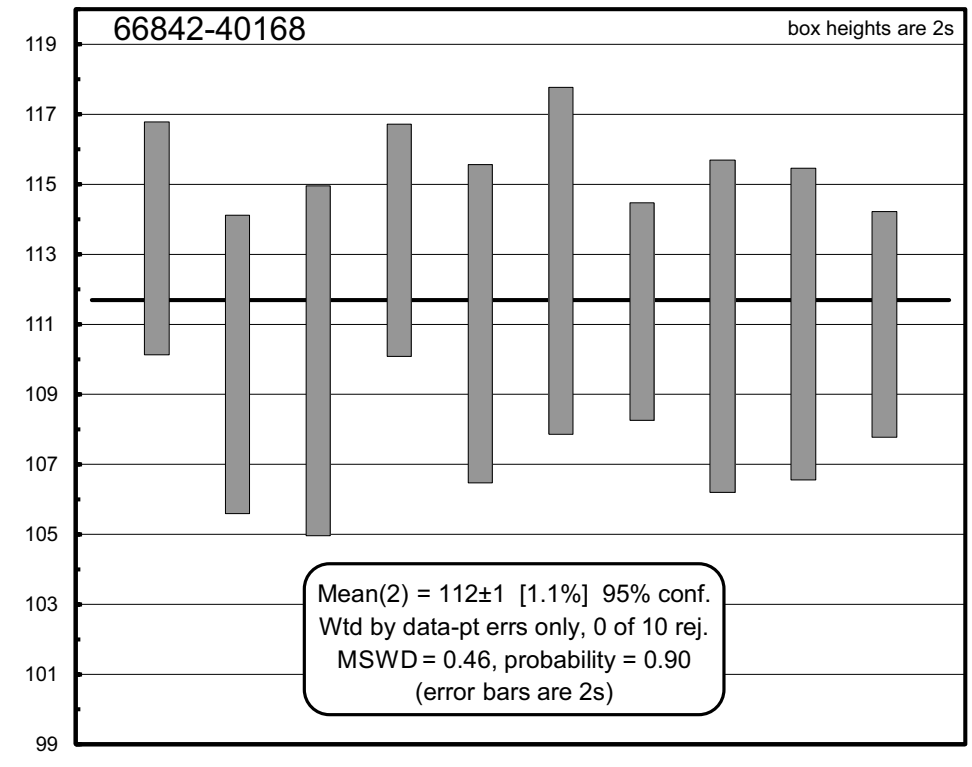
- Granodiorite porphyry dikes
- Intrusive phases:
- phase III: granodiorite
- phase II: quartz monzodiorite, granodiorite
- phase I: diorite
- Major gold-bearing quartz veins and mineralized zones
- Minor veinlets and mineralized zones
- Barren calcite veins
- Sample location

Figure 3

a




b



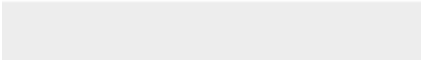



Click here to access/download
Supplementary Material
ESM_Fig1.pdf





Click here to access/download
Supplementary Material
ESM_Fig2.pdf





Click here to access/download
Supplementary Material
ESM_Fig3.pdf



Click here to access/download
Supplementary Material
ESM_Table1.pdf

